Autonomous Control of Inverter-Interfaced Distributed Generation Units for Harmonic Current Filtering and Resonance Damping in an Islanded Microgrid

Wang, Xiongfei; Blaabjerg, Frede; Chen, Zhe

Published in:
I E E E Transactions on Industry Applications

DOI (link to publication from Publisher):
10.1109/TIA.2013.2268734

Publication date:
2014

Document Version
Early version, also known as pre-print

Digital Object Identifier (DOI): 10.1109/TIA.2013.2268734

IEEE Transactions on Industry Applications, Vol. PP, No. 99, Early Access Article, Jun. 2013.

Autonomous Control of Inverter-Interfaced Distributed Generation Units for Harmonic Current Filtering and Resonance Damping in an Islanded Microgrid

Xiongfei Wang
Frede Blaabjerg
Zhe Chen

Suggested Citation

X. Wang, F. Blaabjerg, and Z. Chen, "Autonomous control of inverter-interfaced distributed generation units for harmonic current filtering and resonance damping in an islanded microgrid," *IEEE Trans. Ind. Appl.,* vol. PP, no. 99, Early Access Article, Jun. 2013.

Autonomous Control of Inverter-Interfaced Distributed Generation Units for Harmonic Current Filtering and Resonance Damping in an Islanded Microgrid

Xiongfei Wang, *Member, IEEE,* Frede Blaabjerg, *Fellow, IEEE,* and Zhe Chen, *Senior Member, IEEE*
Department of Energy Technology
Aalborg University, Aalborg, Denmark
xwa@et.aau.dk, fbl@et.aau.dk, zch@et.aau.dk

***Abstract*—Harmonic current filtering and resonance damping have become important concerns in the operation and control of the islanded microgrids. To address these challenges, this paper proposes a control method for the inverter-interfaced Distributed Generation (DG) units, which can autonomously share the harmonic currents and resonance damping burdens. The approach employs a load compensator, which is based on the decomposition of output current, in addition to the outer droop-based power controller as well as the inner voltage and current controllers. The load compensator consists of a virtual fundamental impedance loop for the enhanced reactive power sharing, and a variable harmonic impedance loop which allows to counteract the harmonic voltage drops across the grid-side inductance of DG inverter and also to dampen out harmonic resonance propagation in the microgrid. Lastly, the laboratory tests on a three-phase islanded microgrid setup are carried out to validate the performance of the proposed control scheme.**

I. INTRODUCTION

The microgrid paradigm is emerging as an attractive way to the future smart distribution grids, thanks to its capability to operate in both grid-connected and islanded modes [1]. The dynamic islanding operations bring more flexibility on the integration of Distributed Generation (DG) units, and a provide a more reliable electricity service [2]. On the other hand, in islanded operations, the microgrids usually become much weaker than the traditional distribution grids, owing to the limited capacities of DG sources [3]. Consequently, the harmonic distortion tends to be more apparent in the islanded microgrids [4]. The presence of capacitive household loads, passive harmonic filters, and Power Factor Correction (PFC) capacitors, as well as the parasitic capacitors in distribution feeders can cause the low-order harmonic resonance with the line inductances [5]. Further, a wide spread use of inverters for interfacing DG units also bring harmonic interaction with other devices and even trigger resonances in the microgrid. Depending on the number of the paralleled DG inverters, the resonant frequencies vary in a wide range [6]-[8]. Therefore, the stringent requirements are being imposed on the ancillary services of DG inverters, such as the mitigation of circulating harmonic current, harmonic voltage reduction, and harmonic resonance damping [9], [10].

A number of research efforts have been made to address the aforementioned challenges [11]-[20]. In [11], the idea of Resistive-Active Power Filter (R-APF) is implemented based on a high-bandwidth current controller, where DG inverters are controlled to behave as resistors at harmonic frequencies, such that harmonic resonances and voltage distortions can be damped. To further autonomously share harmonic currents, a droop relationship between the output harmonic power of the DG inverter and the controlled harmonic resistance is built in [12]. However, it has been found that only the output voltage of the DG inverter can be regulated in this way, whereas the voltage at the Point of Connection (PoC) may be undamped when using the *LCL*-filters [13]. The grid-side inductance in the *LCL*-filter can lead to a mismatch between the emulated harmonic resistance and the characteristic impedance of the distribution line [14]. Another popular approach is the virtual output impedance concept, where a load current feedforward loop is introduced together with the output harmonic voltage controller [15]-[18]. This method is essentially a frequency-dependent voltage droop with the load current [18]. Either the virtual inductance or the virtual resistance can be synthesized at the harmonic frequencies. As a consequence, the additional harmonic voltage distortion is inevitable, and can become severe when a large virtual inductance is needed to attenuate the differences among the grid-side inductances in the *LCL*-filters of DG inverters. To alleviate the adverse effect of the grid-side inductance, a PoC voltage feedforward control scheme is reported in [19]. With a positive gain G in the PoC voltage feedforward loop, the harmonic impedance seen from the PoC of the DG unit is scaled down by $1/(1+G)$. But the performance of this scheme is limited to the damping of harmonic resonance, due to the absence of the additional harmonic resistance.

Considering the impact of the grid-side inductance in the *LCL*-filter and the demand of harmonic resonance damping, a Variable Harmonic Impedance (VHI) concept is developed

for single grid-interactive DG inverter [20], which comprises positive resistance and negative inductance at the dominant harmonic frequencies. In this paper, this concept is extended for an islanded microgrid with multiple DG inverters, and an autonomous control method of the DG inverters is proposed for the sharing of harmonic currents and harmonic resonance damping. The approach employs a frequency- and sequence-dependent load compensator that is composed of the Virtual Fundamental Impedance (VFI) and VHI loops. The VFI loop improves the performance of the active power-frequency (P-ω) and reactive power-voltage (Q-V) droop controllers, and mitigates the negative-sequence circulating current [21]. The VHI loop compensates for a portion of grid-side inductance at the dominant harmonic frequencies and achieves a proper sharing of harmonic currents among all the DG inverters. Further, in the presence of harmonic resonance, the VHI loop can shift the resonant points toward a higher frequency range where the harmonic resonance can be more easily dampened. Laboratory test results are shown to validate the performance of the proposed control scheme.

II. Harmonic Current Filtering and Resonance Damping Approaches

This section reviews two autonomous control approaches for harmonic current filtering and resonance damping in an islanded microgrid. The effect of grid-side inductance in the *LCL*-filter of the DG inverter is discussed.

A. System Configuration

Fig. 1 illustrates an example of a low-voltage microgrid dominated by multiple inverter-interfaced DG units. A static switch is used to dynamically disconnect the microgrid from the upstream distribution system during abnormal conditions. For the local and common loads, the diode rectifiers denote the nonlinear loads, while the shunt capacitors represent the capacitive household loads and the parasitic capacitors in the distribution feeders.

During islanded operations, the microgrid voltage usually becomes more distorted due to the limited capacities of DG sources. Also, the presence of shunt capacitors can result in harmonic resonance and propagation in the microgrid. As a consequence, the mitigation of circulating harmonic current among all the DG units is needed to prevent overloading of some DG inverters, and meanwhile, the effective resonance damping measures are also important to suppress harmonic voltage amplifications.

B. R-APF-Based Approach

Fig. 2 illustrates the block diagram of the R-APF-based control approach for the i-th DG unit. The dc-link voltage of the DG inverter is regulated on the energy source side, and is assumed to be constant. The basic idea behind this method is to make the DG inverter operate as a resistor at the harmonic frequencies. It is realized by multiplying the output harmonic voltages of a DG inverter with a conductance, which is then passed through a high-bandwidth current controller [11]. The sharing of harmonic currents in the paralleled DG inverters is achieved by a harmonic var-conductance (H_i-G_i) droop [12].

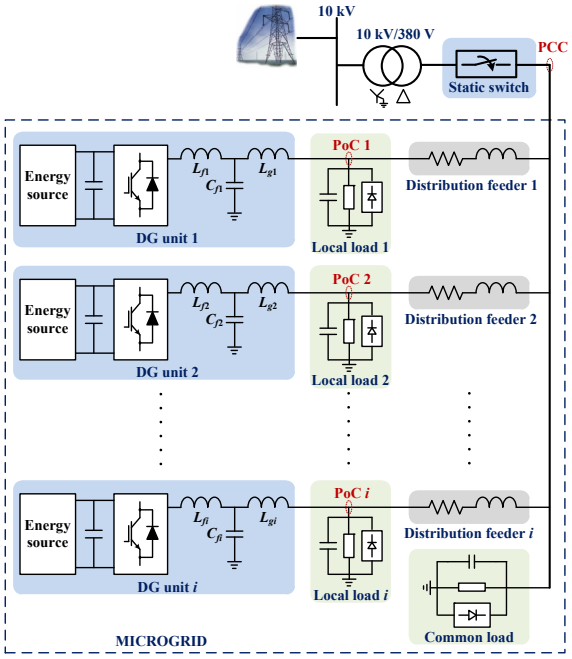

Fig. 1. An example of a low-voltage microgrid dominated with multiple inverter-interfaced DG units.

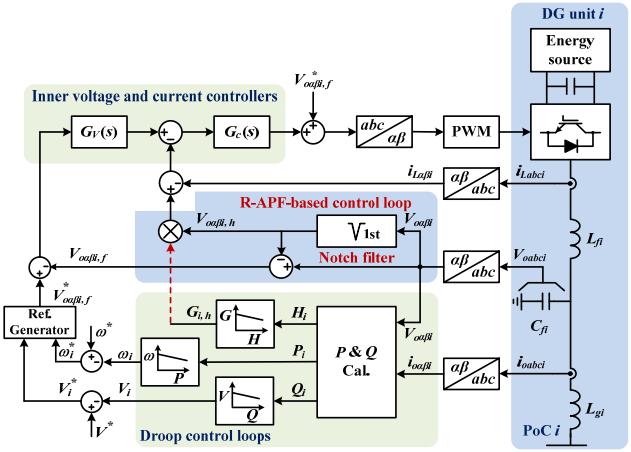

Fig. 2. Control block diagram of the Resistive-Active Power Filter (R-APF)-based approach.

Under this control scheme, Fig. 3 depicts the equivalent circuit of the islanded microgrid at the harmonic frequencies, where nonlinear loads are equivalent to the harmonic current sources for the sake of simplicity. It is worthy to note that the sharing of harmonic current among the DG inverters not only depends on the emulated conductance G_i, but subjects also to the grid-side inductance of the *LCL*-filter, which differs from the islanded network considered in [12]. On the other hand, the grid-side inductance affects the characteristic impedance of the distribution feeder seen at the output of DG inverters, which can cause a mismatch with the emulated conductance and consequently compromise the performance of resonance damping due to the 'whack-a- mole' effect [14].

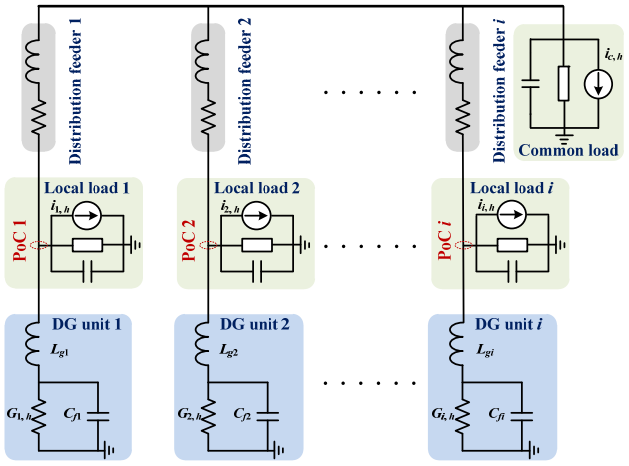

Fig. 3. Equivalent circuit of the islanded microgrid with the R-APF-based approach at the harmonic frequencies.

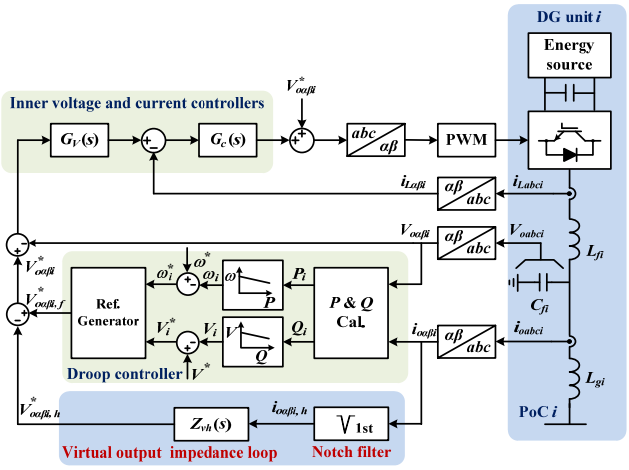

Fig. 4. Control block diagram of the virtual output impedance scheme.

C. Virtual Output Impedance Scheme

Fig. 4 illustrates the control block diagram of the virtual output impedance scheme [15]-[18]. This method essentially builds a frequency-dependent droop relationship between the output harmonic voltage and the output harmonic current of the DG inverter by a load current feedforward loop. A notch filter at the fundamental-frequency is used in the feedforward loop to detect harmonic current. Either the virtual resistance or the virtual inductance can be synthesized [15]-[17]. Thus, the sharing of harmonic current among all the DG inverters is ensured at the expense of the additional harmonic voltages. Consequently, a trade-off between the output voltage quality and the accuracy of harmonic current sharing has to be taken into account in the design of the virtual output impedance.

With the virtual output impedance scheme, Fig. 5 shows the microgrid equivalent circuit at the harmonic frequencies. Similarly, the nonlinear loads are simplified as the harmonic current sources. The paralleled resistance and inductance via the dashed line denote that the DG inverter can be equivalent

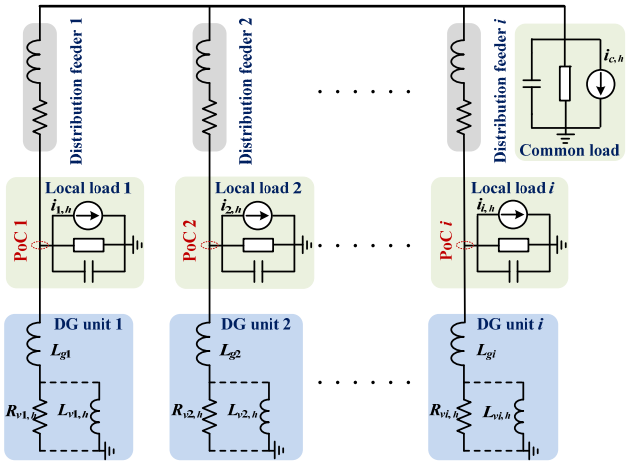

Fig. 5. Equivalent circuit of the islanded microgrid with the virtual output impedance scheme at the harmonic frequencies.

by either the virtual inductance or the resistance. The output capacitors of inverters are absent due to the use of harmonic voltage controllers. Notice that the virtual resistance is more attractive than the inductance, particularly on the damping of harmonic resonance. However, the large grid-side inductance usually requires larger virtual resistance to take effect, which on the other hand leads to more severe harmonic voltages.

III. Proposed Control Method

Fig. 6 shows the block diagram of the proposed control method for the *i*-th DG inverter. This method is based on the multiloop control scheme, where a frequency- and sequence-dependent load compensator that comprises the VFI and VHI loops is developed besides the standard *P*-ω and *Q*-*V* droop controllers, and the inner voltage and current controllers.

Notice that the developed load compensator differs from the conventional virtual output impedance schemes. The VFI loop is split into positive- and negative-sequence impedances at the fundamental-frequency. The positive-sequence VFI is used to enhance the sharing of reactive power by the *Q*-*V* droop, whereas the negative-sequence VFI aims to minimize the negative-sequence circulating current [21]. The VHI loop uses the negative inductance to partially counteract the effect of grid-side inductance at the dominant harmonic frequencies and the positive resistance to realize the autonomous sharing of harmonic currents and harmonic resonance damping.

A. Load Current Decomposer

From Fig. 6, it can be found that the decomposition of the load current is important for realizing the load compensator. A number of power signal decomposition schemes have been developed recently, but the Multiple Synchronous Reference Frames (MSRFs) theory is still considered as one of the best solutions [22].

Fig. 7 shows the block diagram of the MSRFs-based load current decomposer, where the extraction of the positive- and negative-sequence fundamental-frequency currents as well as the dominant harmonic currents is achieved by a set of Park transformations and Low-Pass Filters (LPF).

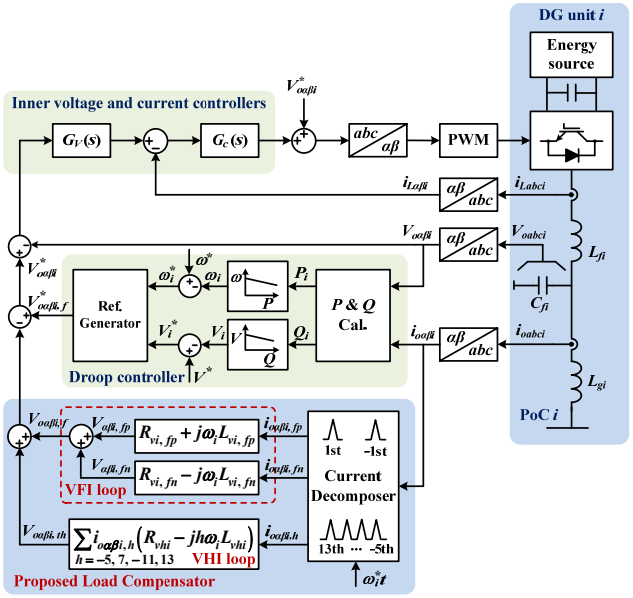

Fig. 6. Block diagram of the proposed control method with a frequency- and sequence-dependent load compensator.

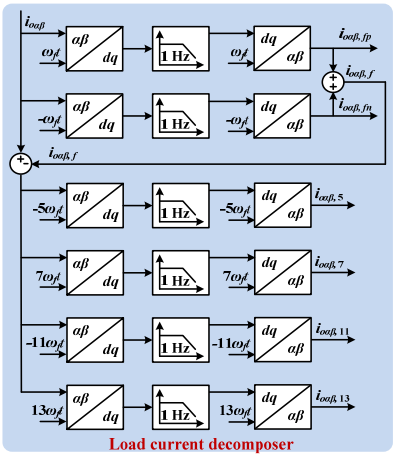

Fig. 7. Block diagram of the MSRFs-based load current decomposer.

The cut-off frequencies of the LPF are designed with the same value as the LPF in the derivation of the average active and reactive power. Thus, the response of VFI loop matches well with the dynamics of the droop-based power controllers and the slope of the *Q*-*V* droop can be dynamically adjusted. Moreover, as the harmonic by definition is a periodic stead-state waveform distortion [23], the cut-off frequency of the LPF for the harmonic current detection can also be chosen as a small value. In this work, the first-order LPF with 1 Hz cut-off frequency is used in the load compensator. However, to further improve the transient performance of the VHI loop, either the higher-order LPF with the higher cut-off frequency [29], or the recursive Park transformation [24] can be used.

B. Design of the VFI and VHI Loops

Fig. 8 depicts the diagrams of the building blocks for the

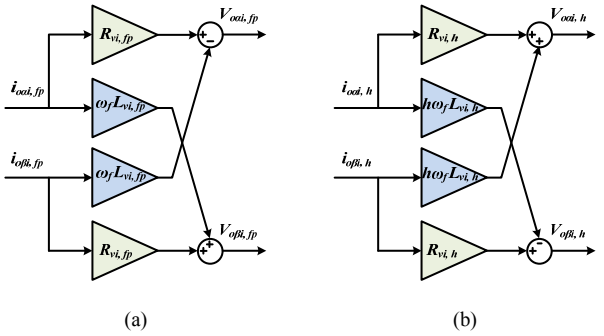

Fig. 8. Diagrams of the building blocks used for realizing (a) the positive-sequence Virtual Fundamental Impedance, and (b) the Variable Harmonic Impedance.

VFI and VHI loops, which can be derived as

$$\begin{pmatrix} V_{o\alpha i,\,fp} \\ V_{o\beta i,\,fp} \end{pmatrix} = \begin{pmatrix} R_{vi,\,fp} & -\omega_f L_{vi,\,fp} \\ \omega_f L_{vi,\,fp} & R_{vi,\,fp} \end{pmatrix} \begin{pmatrix} i_{o\alpha i,\,fp} \\ i_{o\beta i,\,fp} \end{pmatrix} \tag{1}$$

$$\begin{pmatrix} V_{o\alpha i,\,fn} \\ V_{o\beta i,\,fn} \end{pmatrix} = \begin{pmatrix} R_{vi,\,fn} & \omega_f L_{vi,\,fn} \\ -\omega_f L_{vi,\,fn} & R_{vi,\,fn} \end{pmatrix} \begin{pmatrix} i_{o\alpha i,\,fn} \\ i_{o\beta i,\,fn} \end{pmatrix} \tag{2}$$

$$\begin{pmatrix} V_{o\alpha i,\,h} \\ V_{o\beta i,\,h} \end{pmatrix} = \begin{pmatrix} R_{vi,\,h} & h\omega_f L_{vi,\,h} \\ -h\omega_f L_{vi,\,h} & R_{vi,\,h} \end{pmatrix} \begin{pmatrix} i_{o\alpha i,\,h} \\ i_{o\beta i,\,h} \end{pmatrix} \tag{3}$$

where the '*fp*' and '*fn*' represent the fundamental-frequency positive- and negative-sequence components, and '*h*' denotes the dominant harmonic components, which can be -5, 7, -11, and 13. ω_f is the system fundamental-frequency. Notice that the diagram of the negative-sequence VFI is omitted, since it is conjugated to the positive-sequence VFI in Fig. 8 (a).

In the VFI loop, the positive-sequence VFI is designed to be mainly inductive to improve the control of reactive power based on the *Q*-*V* droop [25]. This is because the low-voltage distribution feeders usually have a high R/X impedance ratio, which causes a coupling in the control of active and reactive power when using the conventional droop controllers [2].

The negative-sequence VFI is designed as a resistance to mitigate the negative-sequence circulating current [21]. Due to the component tolerance and parameter drift over time, the unbalanced sensor gains can be present in the DG inverters. As a consequence, the negative-sequence circulating current will arise even in the case of the balanced three-phase loads. Thus, although a balanced three-phase network is built in this work, a large resistance is still synthesized to minimize the undesired negative-sequence circulating current.

The concept of negative inductance has been applied in the excitation system of synchronous generator [26], Flexible AC Transmission System (FACTS) devices [27], [28], as well as the hybrid active filters [29], in order to compensate for a portion of the existing inductance at the fundamental or harmonic frequencies. In this work, the negative inductance in the VHI loop is designed to partially counteract the effect

of the grid-side inductance in the *LCL*-filter of DG inverter. Hence, the negative inductance can be chosen as a portion of the designed grid-side inductance of the *LCL*-filter, and thus the measurement or estimation of the existing impedance can be avoided. Further, the inductor nonlinear behavior also has an important effect on the design of negative inductance. The decrease of inductance due to the saturation may result in the instability of VHI loop. Taking such effect into account, the effective inductance can be expressed as follow [30]

$$\frac{1}{L_{eq}} = \frac{\varphi}{L_{sat}} + \frac{1-\varphi}{L} \tag{4}$$

where L_{eq} is the equivalent inductance, L_{sat} is the saturated inductance, and L is the nominal inductance. φ denotes the proportion of fundamental period for which the inductance is saturated. In order to preserve the stability of the VHI loop, the size of negative inductance needs to be kept smaller than the effective inductance. For the certain saturated inductance, the effective inductance decreases with the reduced duration of saturation. In addition, the harmonic currents generated by the nonlinear inductance can be predicted using the Volterra model and compensated by modifying the harmonic voltage controllers [31], [32].

With the VHI scheme, Fig. 9 shows the equivalent circuit of the microgrid at the dominant harmonic frequencies. It can be found that the harmonic inductance at the PoC of the DG inverter is reduced by the negative inductance in comparison to Fig. 5. Moreover, to ensure the proper sharing of harmonic currents and the effective harmonic resonance damping, the positive resistance in the VHI loop is normally designed as

$$R_{vi,h} >> h\omega_f \left(L_{gi} - L_{vi,h}\right) \tag{5}$$

The larger the resistance, the better the sharing of harmonic currents achieved. On the other hand, with the increase of the resistance, the harmonic voltage at the PoC of DG inverter is increased and the capability of harmonic resonance damping is compromised [12]. Also, the dc-link voltage of the inverter has to be increased. Thus, in the case of harmonic resonance or the presence of waveform-sensitive loads, the resistance is chosen to follow the allowed harmonic voltage limits in [23]

$$i_{i,h} R_{vi,h} \le V^*_{poci,h} \tag{6}$$

where $V^*_{poci,h}$ denotes the individual harmonic voltage limits at the PoC of the DG inverter. Further, the increased harmonic voltages that result from the change of load can be controlled by a centralized harmonic voltage compensator [9], [13]. In respect to the different power capacities of DG inverters for harmonic currents, the positive resistances synthesized by the different DG inverters follow that

$$R_{v1,h} H_1 = R_{v2,h} H_2 = \cdots = R_{vi,h} H_i \tag{7}$$

where H_i is the harmonic power capacity of the ith DG unit.

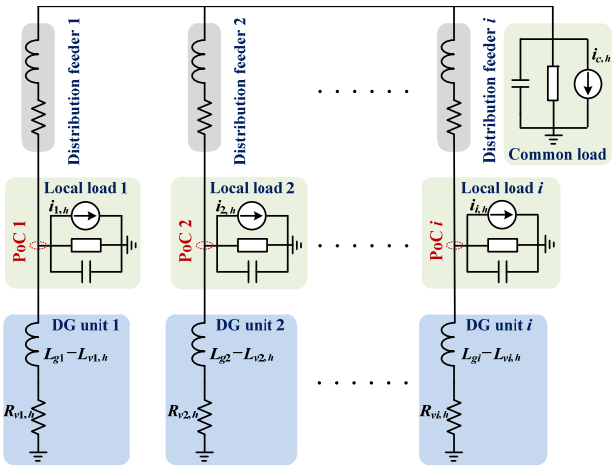

Fig. 9. Equivalent circuit of the islanded microgrid with the VHI loop at the dominant harmonic frequencies.

C. Output Impedance Analysis

It is noted that the dynamic behaviors of the inner voltage and current control loops affect the output impedance profile of a DG inverter, which can be expressed as follows

$$V_o(s) = G_{cl}(s) V_o^*(s) - Z_o(s) I_o(s) \tag{8}$$

$$\begin{aligned} G_{cl}(s) &= \left.\frac{V_o(s)}{V_o^*(s)}\right|_{I_o(s)=0} \\ &= \frac{G_c(s) G_d(s) G_V(s)}{L_f C_f s^2 + \left(G_c(s) G_d(s) + r_f\right) C_f s + G_c(s) G_d(s) G_V(s)} \end{aligned} \tag{9}$$

$$\begin{aligned} Z_o(s) &= \left.\frac{V_o(s)}{I_o(s)}\right|_{V_o^*(s)=0} \\ &= \frac{L_f s + r_f + G_c(s) G_d(s)}{L_f C_f s^2 + \left(G_c(s) G_d(s) + r_f\right) C_f s + G_c(s) G_d(s) G_V(s)} \end{aligned} \tag{10}$$

where $V_o(s)$ and $V_o^*(s)$ are the actual and referenced inverter output voltages, respectively, $G_{cl}(s)$ denotes the closed-loop transfer function of the voltage control loops, and $Z_o(s)$ is the output impedance. r_f is the parasitic resistance of the filter inductance L_f. $G_d(s)$ is the 1.5 sampling period (T_s) delay, which includes the computational delay (T_s) and the PWM delay ($0.5T_s$) [33]. $G_c(s)$ is the proportional inductor current controller, and $G_V(s)$ denotes the capacitor voltage controller with a proportional and multiple resonant integral terms.

$$G_d(s) = \frac{1}{1 + 1.5 T_s s} \tag{11}$$

$$G_V(s) = K_{pv} + \frac{K_{ivf} s}{s^2 + \omega_f^{\,2}} + \sum_{\substack{h=-5,7,\\ -11,13}} \frac{K_{ivh} s}{s^2 + (h\omega_f)^2} \tag{12}$$

Considering the effect of the load compensator, the total output impedance $Z_{to}(s)$ can be derived by

$$Z_{to}(s) = G_{cl}(s)\left(Z_{v,fp}(s) + Z_{v,h}(s)\right) + Z_o(s) \tag{13}$$

$$Z_{v,fp}(s) = \frac{-2\omega_c\omega_f^2 L_{v,fp}}{s^2 + 2\omega_c s + \omega_f^2} \tag{14}$$

$$Z_{v,h}(s) = \sum_{h=-5,7,-11,13} \frac{2\omega_c(R_{v,h}s + (h\omega_f)^2 L_{v,h})}{s^2 + 2\omega_c s + (h\omega_f)^2} \tag{15}$$

where $Z_{v,fp}(s)$ is the positive-sequence VFI and $Z_{v,h}(s)$ is the VHI. Notice that the MSRFs-based load current decomposer can be transformed into the stationary frame by [34]

$$H_{BPF}(s) = H_{LPF}\left(\frac{s^2 + (h\omega_f)^2}{2s}\right) = \frac{2\omega_c s}{s^2 + 2\omega_c s + (h\omega_f)^2} \tag{16}$$

where ω_c is the cut-off frequency of low-pass filters in Fig. 7, 2π rad/s. The effect of negative-sequence VFI is omitted, since it is only for attenuating circulating current.

Fig. 10 gives a comparison between the characteristics of the output impedance $Z_o(s)$ and the total output impedance $Z_{to}(s)$. The parameters of the inverter and designed controller are given in Appendix A. An expanded view of Fig. 10 at both the fundamental and the dominant harmonic frequencies is given in Fig. 11. It is seen that the total output impedance is reshaped by the load compensator, where the fundamental-frequency inductance and the selective harmonic impedances with negative phase angles are synthesized.

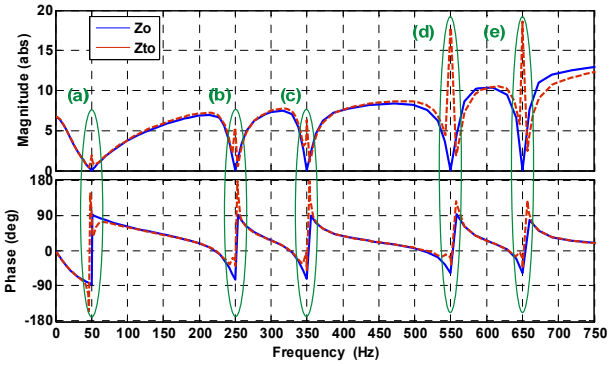

Fig. 10. Comparison between the characteristics of the output impedance $Z_o(s)$ and the total output impedance $Z_{to}(s)$.

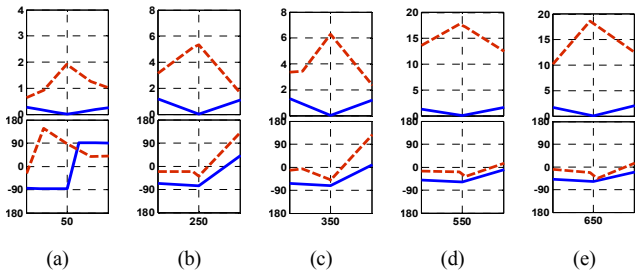

Fig. 11. Expanded view of Fig. 10.

IV. Laboratory Test Results

To confirm the performance of the proposed approach, a three-phase islanded microgrid is built in the laboratory. Fig. 12 shows the hardware picture for the DG inverters and the control platform. Two 5.5 kVA Danfoss frequency inverters are adopted as the DG inverters, which are powered by two constant dc voltage sources, respectively. The control algorithm is applied in the DS1006 dSPACE system with 10.5 kHz sampling frequency and a half-period interrupt shift. The controller parameters and the circuit constants of the microgrid are shown in Appendix A.

Fig. 13 shows a simplified one-line diagram of the built microgrid system. To see the harmonic resonance in the built microgrid, the large shunt-connected capacitors (50 μF) are used to represent the aggregated effect of the capacitive loads, the PFC capacitors, and the parasitic capacitors of the distribution feeders. Two small inductances (0.25 mH) are used to emulate the 1 km, 1 kV cable inductances.

Fig. 14 shows the measured bus voltage waveforms and the associated harmonic spectra without using any harmonic current filtering and harmonic resonance damping schemes. The harmonic spectra are based on the linear RMS values of the phase-A voltages. It can be seen that the fifth harmonic resonance occurs in this test case. Notice that there is not any additional output impedance reshaping loop used other than the output voltage controller. Thus, the enabling of harmonic resonant controllers can reduce the output impedance of the DG inverter at the dominant harmonic frequencies, and cause the struggle of the harmonic controllers in the paralleled DG inverters. The harmonic circulating current will be inevitably increased [15]. Hence, in order to keep a stable operation of the paralleled inverters, the harmonic resonant integrators in the voltage loop need to be kept at zero. The VFI loop keeps active to minimize the negative-sequence circulating current and reactive power difference. Fig. 17 (a) shows the output currents of two inverters and the difference between them in this case. It is observed that the current difference is small due to the presence of large grid-side inductance.

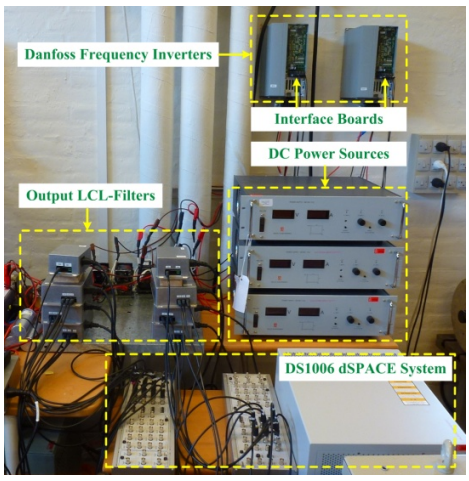

Fig. 12. Hardware picture of the DG inverters and the control platform.

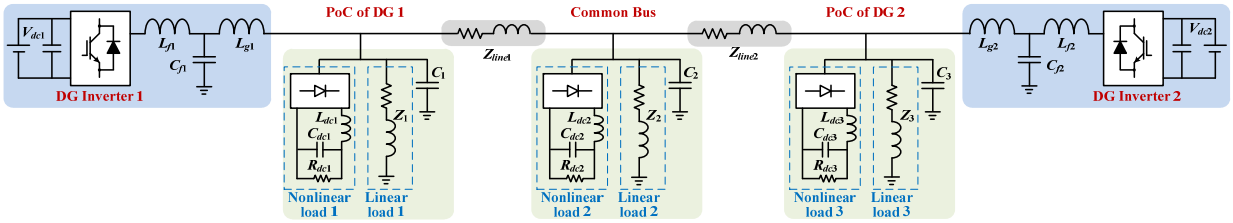

Fig. 13. Simplified one-line diagram of the built three-phase microgrid in laboratory.

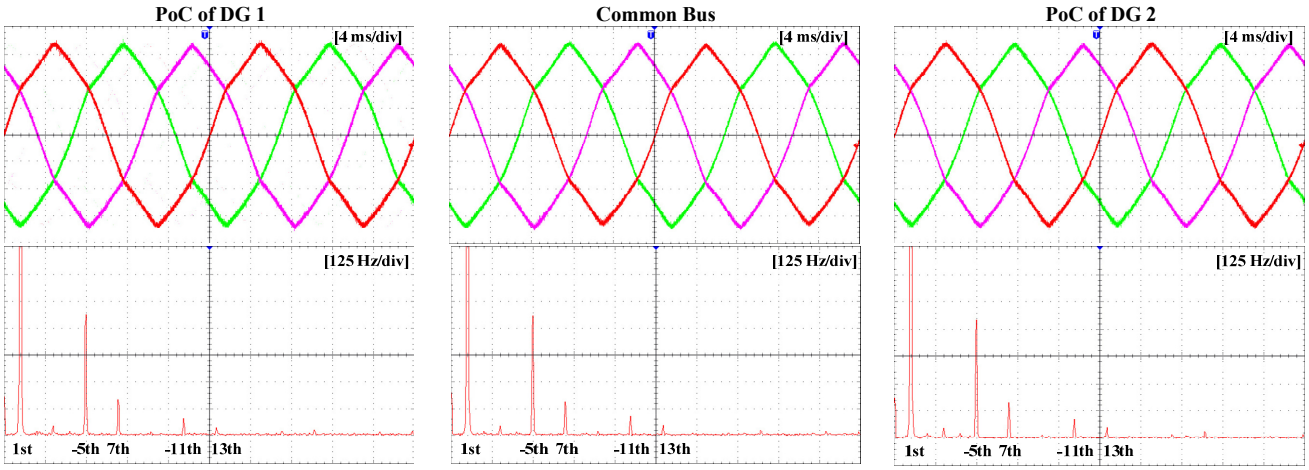

Fig. 14. Measured bus voltage waveforms (100 V/div) and the associated harmonic spectra (2 V_{RMS}/div) without using harmonic current sharing and resonance damping approach.

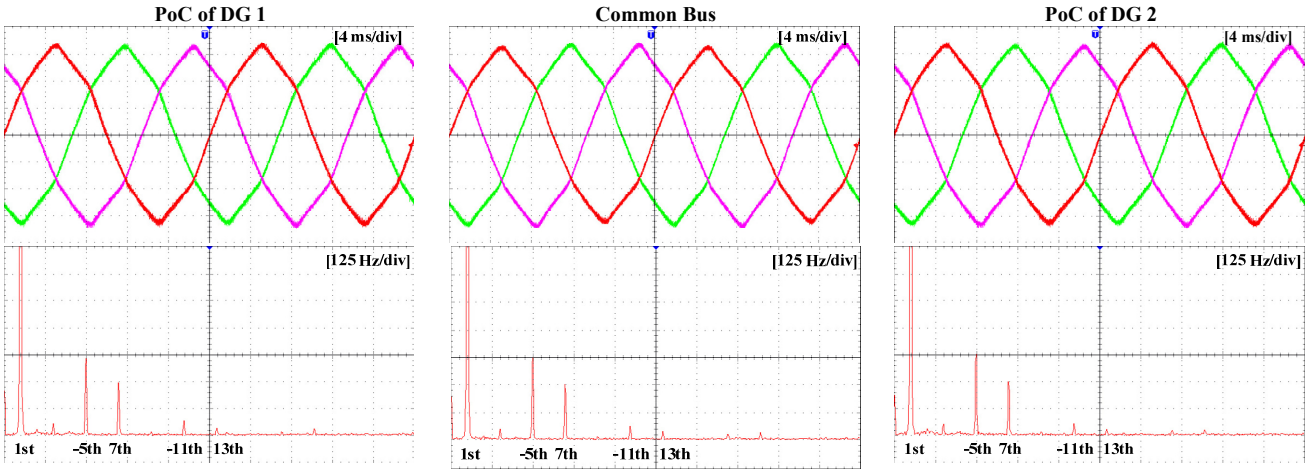

Fig. 15. Measured bus voltage waveforms (100 V/div) and the associated harmonic spectra (2 V_{RMS}/div) with the conventional virtual resistance scheme.

Fig. 15 shows the measured bus voltage waveforms and the associated harmonic spectra with the conventional virtual resistance scheme [16]. In this case, only positive harmonic resistances in the VHI loop are activated. From the harmonic spectra, it is seen that the fifth harmonic voltages are reduced compared to Fig. 14, whereas the seventh harmonic voltages are increased. This indicates the presence of large grid-side inductances may bring a mismatch between the synthesized harmonic resistances and the characteristic impedance of the distribution feeder [14].

Furthermore, from Fig. 17 (b), it can be observed that the output currents of the two inverters become more distorted due to the improvements of the bus voltages. Nevertheless, instead of mitigating the circulating harmonic currents as usual, it can be seen that the output current difference is even increased, which is because the phase angles of equivalent harmonic impedances of two inverters are different.

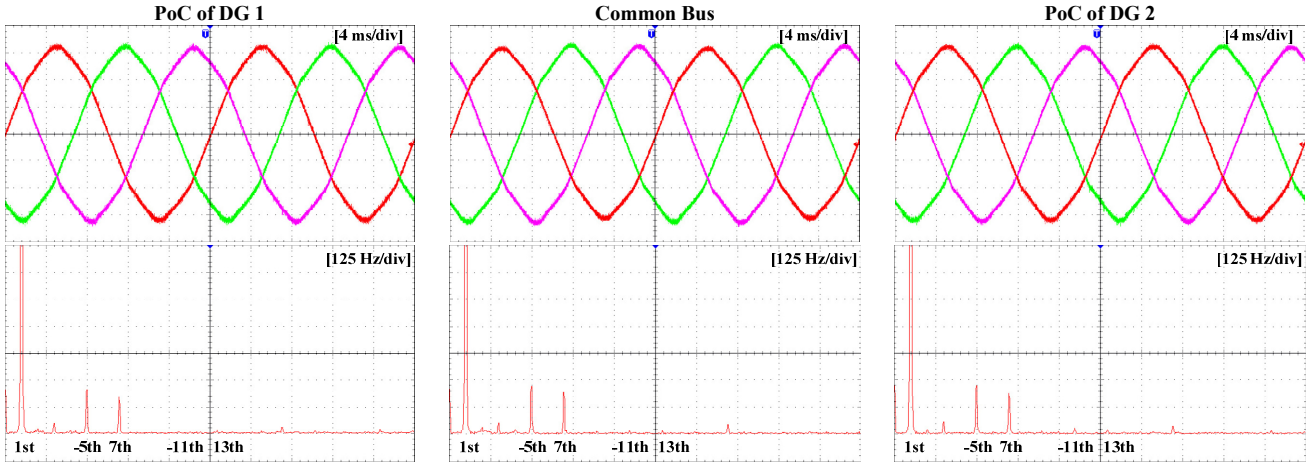

Fig. 16. Measured bus voltage waveforms (100 V/div) and the associated harmonic spectra (2 V_{RMS}/div) with the proposed control method.

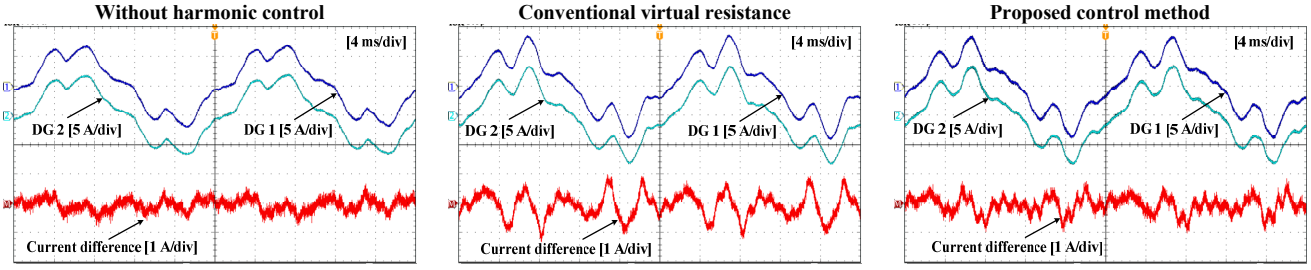

(a) (b) (c)

Fig. 17. Measured output current (Phase-A) waveforms of two DG inverters and the difference between them. (a) Without using harmonic current sharing and resonance damping approach. (b) With the conventional virtual resistance approach. (c) With the proposed control method.

Fig. 16 shows the measured bus voltage waveforms and the associated harmonic spectra with the proposed control method. Compared to Fig. 14 and Fig. 15, it is obvious that the bus voltage waveforms become more sinusoidal. Also, as shown in the harmonic spectra, the fifth harmonic voltages are further damped without increasing the seventh harmonic voltages, which verifies the superior performance of the VHI loop than conventional virtual resistance loop. Table I shows the bus voltage Total Harmonic Distortions (THDs) for the three cases. It is also evident that the bus voltage THDs are effectively reduced with the proposed control method.

Fig. 17 (c) shows the measured output current waveforms using the proposed control method. It is seen that the output currents become more severely distorted, but the current difference is reduced in comparison to Fig. 17 (b). It implies the designed load compensator can achieve harmonic current filtering and resonance damping autonomously.

Fig. 18 shows the measured transient waveforms of two inverters when the nonlinear loads at the PoC of DG 1 and the common bus are switched on. It is seen that the current difference first increases after switching on nonlinear loads, and then drops down to steady-state value. Although the bus voltages become distorted when the nonlinear loads increase, the harmonic resonance is still damped.

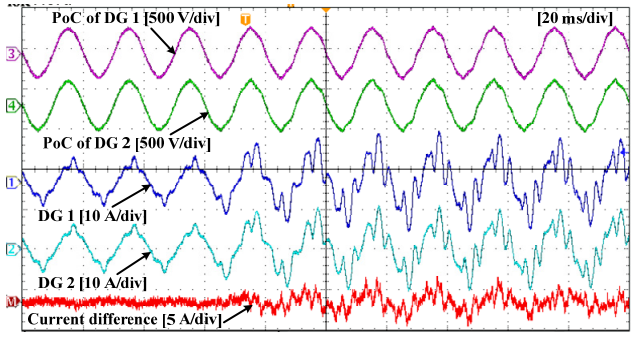

Fig. 18. Measured transient waveforms of two inverters when the nonlinear loads at the PoC of DG 1 and common bus are switched on.

TABLE I. BUS VOLTAGE THDS WITH DIFFERENT CONTROLLERS

Test Case	Voltage THD (%)		
	PoC of DG 1	*Common Bus*	*PoC of DG* 2
Without harmonic control (Fig. 13)	5.2	5.4	5.3
Conventional virtual resistance (Fig. 14)	4.1	4.4	4.2
Proposed control method (Fig. 15)	2.9	3.3	3.1

V. CONCLUSIONS

This paper has discussed harmonic current filtering and resonance damping methods of inverter-interfaced DG units in an islanded microgrid. First, the block diagrams of the R-APF-based approach and the conventional virtual output impedance schemes were presented. The adverse effects of a large grid-side inductance on these two methods have been pointed out. Then, to overcome the problems in the presence of large grid-side inductances, a load compensator including a VFI loop and a VHI loop was proposed. It has been shown that the negative inductances in the VHI loop can effectively counteract the harmonic voltage drops across the grid-side inductance, while the positive harmonic resistances achieve harmonic current filtering and resonance damping. Finally, the laboratory tests of an islanded three-phase microgrid are performed to validate the theoretical analysis and expected performance of the proposed control method.

APPENDIX A

A. Power Stage Parameters of DG Inverters

- Switching frequency: 10.5 kHz
- DC link voltage: $V_{dc1} = V_{dc2} = 780$ V
- AC filter inductor: $L_{f1} = L_{f2} = 1.5$ mH
- AC filter capacitor: $C_{f1} = C_{f2} = 25$ μF
- Grid-side inductor: $L_{g1} = 2$ mH, $L_{g2} = 3$ mH

B. Microgrid Circuit Constants

- System fundamental-frequency: 50 Hz
- Nominal voltage: 380 V
- Distribution feeders: $R_{line1} = R_{line2} = 0.2\ \Omega$
  $L_{line1} = L_{line2} = 0.25$ mH
- Shunt capacitors: $C_1 = C_2 = C_3 = 50$ μF
- Linear loads: $Z_1 = Z_3 = 4.3$ kVA, PF = 0.3
  $Z_2 = 0.3$ kW
- Nonlinear loads: $L_{dc1} = L_{dc2} = L_{dc3} = 84$ μH
  $C_{dc1} = C_{dc2} = C_{dc3} = 235$ μF
  $R_{dc1} = 0.9$ kW, $R_{dc2} = R_{dc3} = 0.6$ kW

C. Proposed Controller Parameters

- Sampling frequency: 10.5 kHz
- Current controller: $K_{pc1} = K_{pc2} = 10$
- Voltage controller: $K_{pv1} = K_{pv2} = 0.15$
  $K_{ivf1} = K_{ivf2} = 120$
  $K_{iv5,1} = K_{iv7,1} = K_{iv11,1} = K_{iv13,1} = 30$
  $K_{iv5,2} = K_{iv7,2} = K_{iv11,2} = K_{iv13,2} = 30$
- Droop controller: $n_{p1} = n_{p2} = 10^{-4}$, $m_{p1} = m_{p2} = 10^{-3}$
- VFI loop: $L_{vfp1} = L_{vfp2} = 6$ mH
  $R_{vfn1} = R_{vfn2} = 20\ \Omega$
- VHI loop: $L_{v5,1} = L_{v7,1} = L_{v11,1} = L_{v13,1} = 1.5$ mH
  $R_{v5,1} = R_{v7,1} = 4\ \Omega$, $R_{v11,1} = R_{v13,1} = 16\ \Omega$
  $L_{v5,2} = L_{v7,2} = L_{v11,2} = L_{v13,2} = 2.25$ mH
  $R_{v5,2} = R_{v7,2} = 4\ \Omega$, $R_{v11,2} = R_{v13,2} = 16\ \Omega$

REFERENCES

[1] R. Lasseter, "Smart distribution: Coupled microgrids," *IEEE Proc.*, vol. 99, no. 6, pp. 1074-1082, Jun. 2011.

[2] X. Wang, J. M. Guerrero, F. Blaabjerg, and Z. Chen, "A review of power electronics based microgrids," *Journal of Power Electron.*, vol. 12, no. 1, pp. 181-192, Jan. 2012.

[3] J. Rocabert, A. Luna, F. Blaabjerg, and P. Rodriguez, "Control of power converters in AC microgrids," *IEEE Trans. Power Electron.*, vol. 27, no. 11, pp. 4734-4749, Nov. 2012.

[4] J. H. Enslin and P. J. Heskes, "Harmonic interaction between a large number of distributed power inverters and the distribution network," *IEEE Trans. Power Electron.,* vol. 19, no. 6, pp. 1586-1593, Nov. 2004.

[5] H. Akagi, H. Fujita, and K. Wada, "A shunt active filter based on voltage detection for harmonic termination of a radial power distribution line," IEEE Trans. Ind. Appl., vol. 35, no. 3, pp. 638-645, May/Jun. 1999.

[6] L. Harnefors, M. Bongiorno, and S. Lundberg, "Input-admittance calculation and shaping for controlled voltage-source converters," *IEEE Trans. Ind. Electron*., vol. 54, no. 6, pp. 3323-3334, Dec. 2007.

[7] J. He, Y. W. Li, D. Bosnjak, and B. Harris, "Investigation and active damping of multiple resonances in a parallel-inverter-based microgrid," *IEEE Trans. Power Electron*., vol. 28, no. 1, pp. 234-246, Jan. 2013.

[8] R. Turner, S. Walton, and R. Duke, "Stability and bandwidth implications of digitally controlled grid-connected parallel inverters," *IEEE Trans. Ind. Electron*., vol. 57, no. 11, pp. 3685-3694, Nov. 2010.

[9] X. Wang, J. M. Guerrero, F. Blaabjerg, and Z. Chen, "Secondary voltage control for harmonic suppression in islanded microgrids," *in Proc. IEEE PESGM* 2011, pp. 1-8.

[10] F. Wang, J. Duarte, M. Hendrix, and P. Ribeiro, "Modelling and analysis of grid harmonic distortion impact of aggregated DG inverters," *IEEE Trans. Power Electron.*, vol. 26, no. 3, pp. 786-797, Mar. 2011.

[11] T. Takeshita and N. Matsui, "Current waveform control of PWM converter system for harmonic suppression on distribution system," *IEEE Trans. Ind. Electron.*, vol. 50, no. 6, pp. 1134-1139, Dec. 2003.

[12] T. Lee, and P. T. Cheng, "Design of a new cooperative harmonic filtering strategy for distributed generation interface converters in an islanding network," *IEEE Trans. Power Electron.*, vol. 22, no. 5, pp. 1919-1927, Sep. 2007.

[13] X. Wang, F. Blaabjerg, Z. Chen, and J. M. Guerrero, "A centralized control architecture for harmonic voltage suppression in islanded microgrids," in *Proc. IEEE IECON* 2011, pp. 3070-3075.

[14] K. Wada, H. Fujita, and H. Akagi, "Considerations of a shunt active fitler based on voltage detection for installation on a long distribution feeder," *IEEE Trans. Ind. Appl.*, vol. 38, no. 4, pp. 1123-1130, Jul./Aug. 2002.

[15] U. Borup, F. Blaabjerg, and P. Enjeti, "Sharing of nonlinear load in parallel-connected three-phase converters," *IEEE Trans. Ind. Appl.*, vol. 37, no. 6, pp. 1817-1823, Nov./Dec. 2001.

[16] D. De and V. Ramanarayanan, "Decentralized parallel operation of inverters sharing unbalanced and non-linear loads," *IEEE Trans. Power Electron.*, vol. 25, no. 12, pp. 1126-1132, Dec. 2010.

[17] T. Vandoorn, B. Meersman, J. D. Kooning, and L. Vandevelde, "Controllable harmonic current sharing in islanded microgrids: DG units with programmable resistive behavior toward harmonics," *IEEE Trans. Power Del.*, vol. 27, no. 2, pp. 831-841, Apr. 2012.

[18] S. J. Chiang and J. M. Chang, "Parallel control of the ups inverters with frequency-dependent droop scheme," in *Proc. IEEE PESC* 2001, pp. 957-961.

[19] J. He, Y. W. Li, and M. S. Munir, "A flexible harmonic control approach through voltage-controlled DG-grid interfacing converters," *IEEE Trans. Ind. Electron.*, vol. 59, no. 1, pp. 444-455, Jan. 2012.

[20] X. Wang, F. Blaabjerg, and Z. Chen, "Synthesis of variable harmonic impedance in inverter-interfaced distributed generation unit for harmonic resonance damping throughout a distribution network," *IEEE Trans. Ind. Appl.*, vol. 48, no. 4, pp. 1407-1417, Jul./Aug. 2012.

[21] X. Wang, F. Blaabjerg, and Z. Chen, "An improved virtual impedance for droop-controlled parallel three-phase voltage source inverters," in *Proc. IEEE ECCE* 2012, pp. 2466-2473.

[22] V. Moreno, M. Liserre, A. Pigazo, and A. Dell'Aquila, "A comparative analysis of real-time algorithms for power signal decomposition in multiple reference frames," *IEEE Trans. Power Electron.*, vol. 22, no. 4, pp. 1280-1289, Jul. 2007.

[23] *IEEE Recommended Practice and Requirements for Harmonic Control in Electrical Power Systems,* IEEE Std. 519-1992, 1992.

[24] A. Pigazo, V. M. Moreno, and E. J. Estebanez, "A recursive Park transformation to improve the performance of synchronous reference frame controllers in shunt active power filters," *IEEE Trans. Power Electron*., vol. 24, no. 9, pp. 2065-2075, Sep. 2009.

[25] J. He and Y. W. Li, "Analysis, design, and implementation of virtual impedance for power electronics interfaced distributed generation," *IEEE Trans. Ind. Appl.*, vol. 47, no. 6, pp. 2525-2538, Nov./Dec. 2011.

[26] *IEEE Recommended Practice for Excitation System Models for Power System Studies*, IEEE Std. 421.5-1992, 1992.

[27] D. M. Divan, "Non dissipative switched networks for high power applications," *Electron. Lett*., vol. 20, no. 7, pp. 277-279, Mar. 1984.

[28] H. Funato, A. Kawamura, and K. Kamiyama, "Realization of negative inductance using variable active-passive reactance (VAPAR)," *IEEE Trans. Power Electron*., vol. 12, no. 4, pp. 589-596, Jul. 1997.

[29] S. Bhattacharya, P. T. Cheng, and D. M. Divan, "Hybrid solutions for improving passive filter performance in high power applications," *IEEE Trans. Ind. Appl*., vol. 33, no. 3, pp. 732-747, May/Jun. 1997.

[30] D. H. Boteler, "Characteristics of time-varying inductance," *IEEE Trans. Magn*., vol. 30, no. 2, pp. 172-176, Mar. 1994.

[31] R. A. Mastromauro, M. Liserre, and A. Dell'Auila, "Study of the effects of inductor nonlinear behavior on the performane of current controllers for single-phase PV grid converters," *IEEE Trans. Ind. Electron*., vol. 55, no. 5, pp. 2043-2052, May 2008.

[32] F. Yuan and A. Opal, "Distortion analysis of periodically switched nonlinear circuits using time-varying Volterra series," *IEEE Trans. Circuits Syst. I, Fund. Theory Appl*., vol. 48, no. 6, pp. 726-738, Jun. 2001.

[33] V. Blasko and V. Kaura, "A new mathematical model and control of a three-phase AC-DC voltage source converter," *IEEE Trans. Power Electron.*, vol. 12, no. 1, pp. 116-123, Jan. 1997.

[34] D. N. Zmood and D. G. Holmes, "Stationary frame current regulation of PWM inverters with zero steady-state error," *IEEE Trans. Power Electron.*, vol. 18, no. 3, pp. 814-822, May 2003.